Structural Eng./Earthquake Eng., JSCE, Vol. 18, No. 1, 1s−11s, 2001 January
(J. Struct. Mech. Earthquake Eng., JSCE, No. 668/ I−54)

CRACKING AND FAILURE BEHAVIOR OF CONCRETE TUNNEL LINING PREDICTED BY SMEARED CRACK MODEL

Jun YIN[1], Zhishen WU[2], Toshihiro ASAKURA[3] and Hiroyuki OTA[4]

[1]Student Member of JSCE, MS of Eng. Dept. of Urban & Civil Eng., Ibaraki University
(Nakanarusawa-cho 4-12-1, Hitachi Ibaraki 316-8511, Japan)
[2]Member of JSCE, Dr. of Eng., Associate Professor, Dept. of Urban & Civil Eng., Ibaraki University
(Nakanarusawa-cho 4-12-1, Hitachi Ibaraki 316-8511, Japan)
[3]Member of JSCE, Dr. of Eng., Associate Professor, Dept. of Earth Resource Eng., Kyoto University
(Yoshida-honmachi, Sakyo-ku, Kyoto-ku, Kyoto-shi, Kyoto 606-01, Japan)
[4]Member of JSCE, OYO Technical Center, OYO Corporation
(Toro-cho 2-61-5, Omiya, Saitama 330-0034, Japan)

In this paper, the cracking behavior of concrete tunnel lining is simulated by a finite element code with smeared crack model. Based on the experimental observation, numerical simulations are carried out in the following aspects: 1)initial imperfection; 2)concrete tensile strength; 3)fracture energy; 4)load direction; 5)size effect on structural strength and 6)soil mass constrain. The analyses on the items of 1) through 3) treat the basic factors affecting the cracking behavior of tunnel lining. And studies of 4) through 6) can provide a better understanding of tunnel lining response under complicated conditions.

Key Words: concrete tunnel lining, softening, cracking, smeared crack model, structural strength

1. INTRODUCTION

In Japan, there are 4600 railway tunnels with a total length of 2900km and 6500 road tunnels with a total length of 1800km in practical service. Many of them have been in service for decades of years, among which about half of the railway tunnels were built before World War II. In addition, Japan is a narrow island country with large coverage of mountains and uneven topographic features. Tuff and mud rocks generated during Neogene Period are soft with low strength and are widely distributed in Japan. These kinds of geologic defects have been also disadvantageous to the normal service of tunnels. Therefore, there exist serious problems of how to efficiently inspect, diagnose and repair them to extend the service life.

Although these problems have drawn much attention of designers and researchers in the engineering field and some measurements have been applied to the practical use, many current methods for evaluating the conditions of the existing tunnel linings are still on the stage of qualitative analysis. More extensive studies and comprehensive understanding of cracking behavior of tunnel linings have become more necessary to establish a proper standard of designing the new tunnel linings and of maintaining the existing ones under various service conditions. In recent years, the scale model experiments[1), 4)] have been done to study the mechanism of tunnel deformation and the reinforcing effect of externally bonded fiber plastics sheets or steel plates, through which much valuable data have been obtained. However, the experimental method alone is still far from sufficiency. It is difficult to simulate some complicated cases. Hence, the analysis with some proper numerical models[2)] is becoming an indispensable tool.

In the present paper, the smeared crack model is used in the finite element code for simulating the cracking behavior of plain concrete tunnel linings. The main objective of this study research is to obtain a basic understanding of the cracking behavior of plain concrete tunnel linings, including cracking occurrence and propagation, and

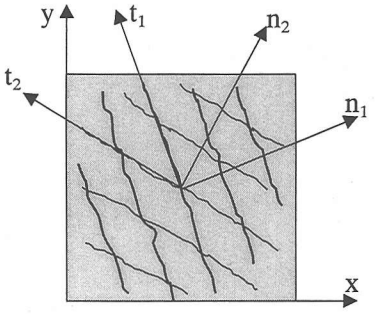

Fig.1 Smeared multiple crack model

discussion of the factors affecting the cracking behavior and the structural responses. The analytical results could provide a reference to the design and maintenance of tunnel linings.

2. SMEARED CRACK MODEL

Smeared crack model has been widely used to simulate the crack behaviors of concrete in the past decades. The fundamental assumption of smeared crack model is a decomposition of total strain increment into a continuous concrete strain increment $\Delta\boldsymbol{\varepsilon}^{co}$ and a crack strain increment $\Delta\boldsymbol{\varepsilon}^{ck}$:

$$\Delta\boldsymbol{\varepsilon} = \Delta\boldsymbol{\varepsilon}^{co} + \Delta\boldsymbol{\varepsilon}^{ck} \tag{1}$$

As proposed by de Borst and Nauta[3], the crack strain increment $\Delta\boldsymbol{\varepsilon}^{ck}$ may further be divided into several components for the strain increment owing to a primary crack, a secondary crack, and so on, as shown in **Fig.1**. The relation between the strain increment in global coordinates and the crack strain increment in local coordinate aligned with the cracks may be written as:

$$\Delta\boldsymbol{\varepsilon}^{ck} = \boldsymbol{N}\,\Delta\boldsymbol{e}^{ck} \tag{2}$$

in which $\boldsymbol{N}$ is a strain transforming matrix containing each sub-transforming matrix of individual local crack strain increment in $\Delta\boldsymbol{e}^{ck}$ to the global coordinates. A stress vector $\Delta\boldsymbol{s}$ assembles all the stress increments with respect to their own local coordinate system. And the relation between the stress increment $\Delta\boldsymbol{\sigma}$ in global coordinate system and the stress vector $\Delta\boldsymbol{s}$ can be derived to be

$$\Delta\boldsymbol{s} = \boldsymbol{N}^{T}\,\Delta\boldsymbol{\sigma} \tag{3}$$

To create a general relationship between the stress increment $\Delta\boldsymbol{\sigma}$ and total strain increment $\Delta\boldsymbol{\varepsilon}$, we firstly assume:

$$\Delta\boldsymbol{\sigma} = \boldsymbol{D}^{co}\,\Delta\boldsymbol{\varepsilon}^{co} \tag{4}$$

with the matrix $\boldsymbol{D}^{co}$ containing the variable modulus of concrete since analyses can be performed with elastoplastic and visco-elastic concrete properties. But presently, $\boldsymbol{D}^{co}$ is simply regarded as the elastic matrix.

In the similar manner, the relation between the crack strain increment $\Delta\boldsymbol{e}^{ck}$ and the stress increment $\Delta\boldsymbol{s}$ can be defined as

$$\Delta\boldsymbol{s} = \boldsymbol{D}^{ck}\,\Delta\boldsymbol{e}^{ck} \tag{5}$$

where $\boldsymbol{D}^{ck}$ is an assembling matrix that contains all the matrices $\boldsymbol{D}_n^{ck}$ (n=1,2,3,...) for each local stress-strain relation of cracked concrete. For an individual crack n, the stress-strain relation is simplified as

$$\boldsymbol{D}_n^{ck} = \begin{bmatrix} \boldsymbol{D}^{I} & 0 \\ 0 & \boldsymbol{D}^{II}\,(or\,\boldsymbol{D}_0^{II}) \end{bmatrix} \tag{6}$$

in which D^I is mode I tensile softening modulus, D^{II} is mode II shear softening modulus and D_0^{II} is the initial shear modulus before the mode II softening is entered.

For the smeared crack model in the sense of crack band theory, the actual crack discontinuity, δ_n for opening and δ_t for sliding, are smeared over the a band of width h. Therefore, the crack strains $e^{ck}=\delta_n/h$ and $\gamma^{ck}=\delta_t/h$ are obtained. In the simple form, the crack band width h can be taken as the equivalent element size, e.g., for 2-dimension elements as $h=\sqrt{A}$, where A is the element area. Fracture energy is assumed to be a material property, which is defined as the amount of energy needed to create a unit area of crack. The areas below the local stress-strain curves at crack interface are the unit fracture energy over crack band h, G_f^I/h for mode I and G_f^{II}/h for mode II,

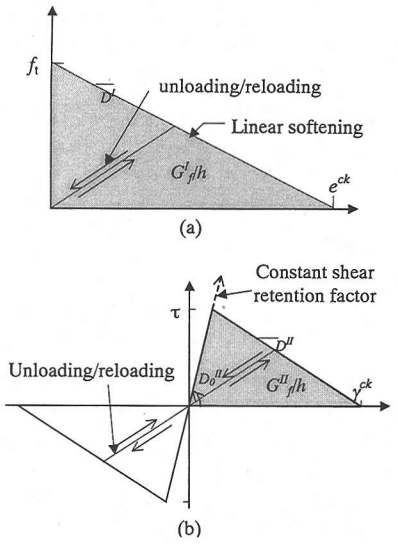

Fig. 2 (a) Mode I tensile softening
(b) Mode II shear softening

respectively, as shown in **Fig.2.**

In this paper, the linear curve for tension softening is used. It is assumed that mode I fracture is initiated firstly when principle stress reaches the tensile strength. Therefore, the shear stress across the crack is zero at the onset of cracking, which is why the shear softening diagram in Fig.2 starts in the origin. Upon subsequent change of the principle stress axes the shear stress across the initial interface may increase until its maximum value τ, thereafter the shear softening branch is started. Different from the present treatment of mode II softening, in the traditional smeared crack model, a constant shear retention factor β is multiplied to the elastic shear modulus and kept unchanged in subsequent calculation. That will easily result in shear stress locking so as to lead to incorrect numerical results. The comparison of the softening model used in this paper and traditional retention factor method for post-crack shear modulus treatment along the crack interface is discussed in section 4.

Furthermore, the unloading and reloading behaviors have been modeled by a secant path, which implies that the stress follows a linear path back to the origin. This procedure is applied to both tensile stress and shear stress. Since no coupling between mode I and mode II is considered, it is easy to trace the softening, unloading and reloading

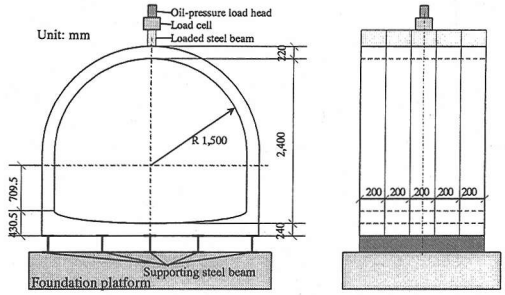

Fig.3 1/3 scale model of tunnel lining

of mode I and mode II separately.

Using Equation (1) through (5), the incremental stress-strain relationship in the global coordinate system for cracked concrete can be developed as

$$\Delta\boldsymbol{\sigma} = [\boldsymbol{D}^{co} - \boldsymbol{D}^{co}\boldsymbol{N} (\boldsymbol{D}^{ck} + \boldsymbol{N}^T\boldsymbol{D}^{co}\boldsymbol{N})^{-1}\boldsymbol{N}^T\boldsymbol{D}^{co}]\Delta\boldsymbol{\varepsilon} \quad (7)$$

It is convenient to be implemented to the finite element code.

3. REVIEW OF EXPERIMENTS

In the experiment, the 1/3 scale model of plain concrete tunnel lining, as shown in **Fig.3**, was tested. The tunnel lining was supported by I-shaped steel beams. No soil mass constrain outside the sidewalls was simulated. The external load was acted vertically down at the outside crown, which was transferred by a steel beam from the oil pressure load machine to the tunnel lining specimen. This kind of load condition approximated the 2-dimension case. The displacement in the experimental load-displacement curves denotes the vertical deformation of load point.

The material properties identified by cylinder specimen under uniaxial compression are uniaxial compressive strength f_c = 262kgf/cm^2, Young's modulus E=2.3×10^{5}kgf/cm^2 and Poisson ratio ν=0.17[4]. As a reference property, the tensile strength f_t can be calculated through transformation equation f_t=0.5$f_c^{2/3}$=20.5kgf/cm^2, based on the concrete design standard of JSCE.

According to the experimental observation[4], the first crack occurred in the crown (inside) followed by the inside cracks at the bottom and outside cracks at the sidewalls in **Fig.4**. Although the

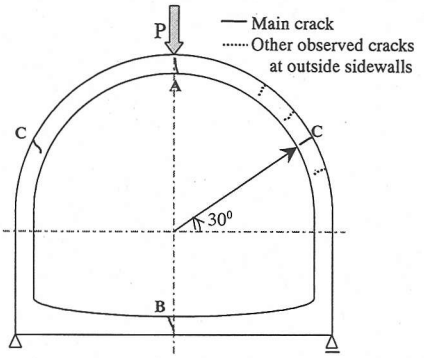

Fig.4 Cracks observed in experiments

second largest moment, besides the inside of crown, is located at the position of the sidewalls at around 30^0 inclined to horizontal direction, the cracks at other positions, such as at 25^0, 40^0 and 50^0, were also observed. This may be due to 1)strength variety and uncertainty resulting from the inhomogeneous behavior of concrete; 2)gentle moment distribution along the sidewall.

The structural deformation increased immensely after the crack occurred at the inside of crown. But the tunnel lining could still resist the external load until the cracks happened at the outside of sidewalls. When the cracks at the sidewalls propagated to a certain extent, the tunnel lining began to lose its load resistance with the continuous deformation up to the ultimate collapse. Two experimental data are shown in **Fig.5**. The difference between Exp.1 and Exp.2 may be due to the randomness and uncertainty of concrete during casting and curing the specimens. A possible reason of the zigzag behavior in Exp.1 might result from the relatively low stiffness of testing machine. Therefore, the displacement control could not be well performed. In order to compare with the static numerical simulation, the dash envelope curve as an idealized load-displacement curve under displacement control is shown in the **Fig.5**. It can be seen that the structural response can be divided into four stages: 1)elastic stage with constant stiffness; 2)nonlinear stage after cracking occurrence with gradually decreased stiffness (but still positive); 3)strength degradation stage with negative stiffness; 4)ultimate structural collapse.

4. NUMERICAL SIMULATIONS

In this section, the smeared crack model that is

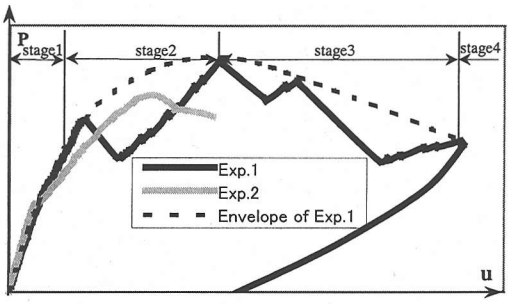

Fig.5 Four stages of tunnel lining response

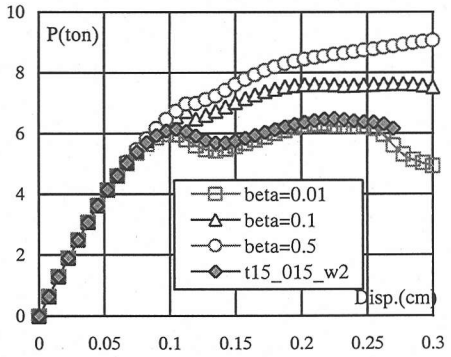

Fig.6 Different treatments of shear modulus

implemented in a finite element code, is used to simulate the cracking behavior of plain concrete tunnel lining. A 4-node plane stress element is used to discritize the tunnel lining, which is integrated at 4 Gaussian quadratic points. The displacement in all the load-displacement figures of numerical simulation denotes the load point displacement.

Before the numerical simulation of tunnel linings, firstly, the difference between the proposed mode II shear softening model and the traditional constant shear retention factor is studied. The constant shear retention factor with β =0.5, 0.1 and 0.01 is used respectively for the traditional post-tension crack treatment of shear modulus. The results, as shown in **Fig.6**, are compared with the one of the shear softening model with initial shear retention factor with β =0.5, shear strength τ =2.0kgf/cm^2 and mode II fracture energy G^{II}_f=0.01kgf/cm, **Fig.2(b)**. The intercrack threshold angle is set 60^0 [3].

It is demonstrated that value of constant shear retention factor significantly influences the numerical results even though the mode II fracturing is not dominant in the tunnel lining structure under such a load condition. Only the result with β =0.01 is similar to the one of the

Table 1 Numerical simulation cases

Numerical Simulation Cases	Tensile strength f_t (kgf/cm^2)	Mode I G^I_f (kgf/cm)	Position of Imperfection	Load Direction , Inclined to x	Size Scale	Soil Mass Stiffness c (kgf/cm^2)
t12_02_w2*	12.0	0.20	①+②	90^0	1/3	
t12_02	12.0	0.20		90^0	1/3	
t12_02_w	12.0	0.20	①	90^0	1/3	
t12_02_w2_p1	12.0	0.20	①+③	90^0	1/3	
t12_02_w2_p2	12.0	0.20	①+④	90^0	1/3	
t10_02_w2	10.0	0.20	①+②	90^0	1/3	
t18_02_w2	18.0	0.20	①+②	90^0	1/3	
t12_01_w2	15.0	0.10	①+②	90^0	1/3	
t12_03_w2	15.0	0.30	①+②	90^0	1/3	
t15_015_w2_L0	15.0	0.15	⑤+⑥	0^0	1/3	
t15_015_w2_L7.5	15.0	0.15	⑤+⑬	0^0	1/3	
t15_015_w2_L30	15.0	0.15	⑤+⑦+⑧	30^0	1/3	
t15_015_w2_L45	15.0	0.15	⑤+⑨+⑩	45^0	1/3	
t15_015_w2_L60	15.0	0.15	⑤+⑪+⑫	60^0	1/3	
t15_015_w2**	15.0	0.15	①+②	90^0	1/3	
t15_015_w2_f	15.0	0.15	①+②	90^0	1	
t15_015_w2_s10	15.0	0.15	①+②	90^0	1/10	
t15_015_w2_s20	15.0	0.15	①+②	90^0	1/20	
t15_015_w2_s30	15.0	0.15	①+②	90^0	1/30	
t15_015_w2_c15	15.0	0.15	①+②	90^0	1/3	15
t15_015_w2_c35	15.0	0.15	①+②	90^0	1/3	35

* and ** denote the basic cases in numerical simulation compared with other cases. The details of different cases appeared in Table 1 are described and shown in figures of each sub-section.

shear softening model, by which the shear stress locking is greatly reduced. In the viewpoint of concrete material behavior, the shear softening model is more physically reasonable because concrete is quasi-brittle material and the shear modulus dose not likely drop dramatically at the onset of the crack opening. In the following simulations, the mode II softening model is adopted.

Due to the structural complexity of the tunnel lining, several factors are involved to affect the cracking behavior of tunnel lining. Six aspects are discussed as follows: 1)effect of initial imperfection for modeling the strength variety and uncertainty of concrete; 2)effect of concrete tensile strength; 3)effect of concrete fracture energy; 4)effect of loading direction; 5)size effect on structural strength and 6)effect of soil mass constrain. The analyses of 1) through 3) are mainly concerned with the basic investigation and give a brief understanding of cracking behavior of the tunnel lining. Analysis 4) extends to the simulation of more general cases with various load conditions. It is helpful to know what kind of load may most possibly cause the failure that could happen in realistic tunnel linings. Analysis 5) tries to find the relationship of structural response among the different size scales of models. And in 6), the effect of outside soil mass constrain on tunnel lining response is considered.

The constant material properties of concrete are taken as Young's modulus $E=1.2\times10^5$kgf/cm^2 for 1), 2), 3), which are identified from FEM calculation according to the elastic behavior of experimental results of 1/3 scale model even though it is different from the experimental value of the concrete sample, and $E=1.4\times10^5$kgf/cm^2 for 4), 5), 6), Poisson ratio $\nu=0.17$. Considering that the tensile crack is primary and the shearing crack is relatively less dominant, the shear strength $\tau=2$kgf/cm^2 and fracture energy for mode II $G^{II}_f=0.01$kgf/cm are kept constant in all the simulation cases. The tensile

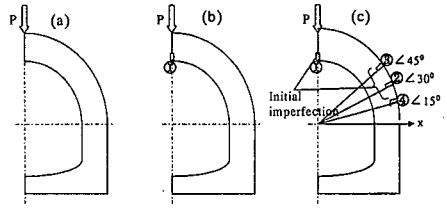

Fig.7 Cases with different initial imperfections

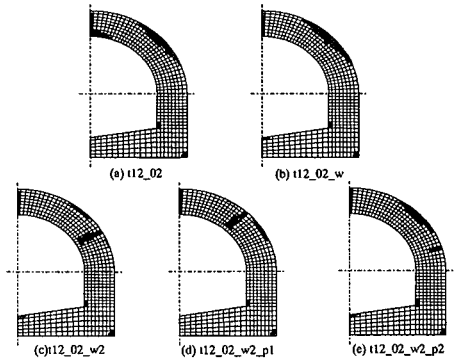

Fig.8 Crack patterns of with and without initial imperfections

strength f_t in the simulation is also determined through elastic stage simulation. It is found that choosing the tensile strength obtained from the concrete sample in simulation would overestimate the structural strength. It will be discussed in the following subsection. Since the value of the mode I concrete fracture energy G_f^I was not identified from the experiment and it is also difficult to be measured accurately, it is considered as a parameter in the case study. The details of the case study are shown in **Table 1**.

(1) Initial Imperfection Effect

From the experimental observations, the cracks are mainly localized at the following positions: 1)inside of crown, 2)outside of sidewalls, and 3)bottom of tunnel. It is also found that the load bearing capacity of tunnel lining degrades after a crack occurs and starts to propagate.

Five cases are studied for the effect of the initial imperfection, as shown in **Fig.7**: **Fig.7(a)** without any initial imperfection, **Fig.7(b)** with initial imperfection only at inside crown and three cases of different initial imperfection positions ①+②, ①+③, ①+④ in **Fig7(c)**. The initial imperfection is assigned by weak elements with only 1/2 concrete tensile strength and 1/4 fracture energy G_f^I as the normal ones.

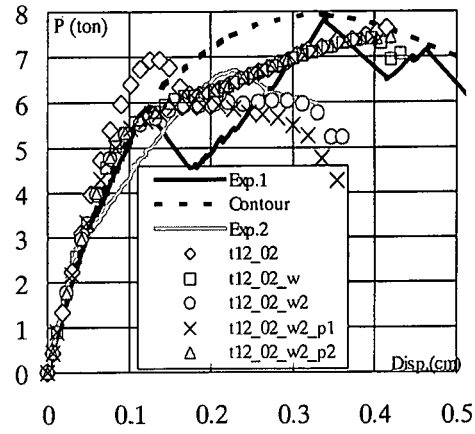

Fig.9 Load-displacement relation with and without initial imperfections

The numerical results of crack patterns and load-displacement curve are shown in **Fig.8** and **Fig.9**, respectively. For plain concrete, the crack localization behavior is very common. However, it can be found that if no initial imperfection is given to the tunnel linings, **Fig.8(a)** and **Fig.8(b)**, the cracks are widely distributed at the outside of sidewalls, but not localized at the position②in **Fig.7**, where the largest stress occurs. This may result from two reasons. One comes from the deficiency of the smeared crack model, which treats the cracks by distributing the stiffness lose through the whole area of a finite element, but not on the crack interface. This easily leads to the distributed crack at the structural level. And the second reason may be due to the structural features of tunnel lining and the material behavior of concrete. Under the vertical load, the stress gradient along the outside of sidewalls is very small. In finite element simulation, generally once one element happens to crack and begins to enter softening, the surrounding elements should have followed an elastic unloading path. But due to the small stress gradient, the surrounding elements may also crack simultaneously so that the crack localization would not be reflected well unless the increment is very small. To avoid such problems, weak elements at some critical positions are given in tunnel linings. This remedy seems to be effective in the present analysis of cracking behavior of concrete tunnel lining.

From **Fig.9**, the obvious ultimate strength degradation is manifested only in cases of t12_02_w2 and t12_02_w2_p1, which have obvious crack localization and whose results are

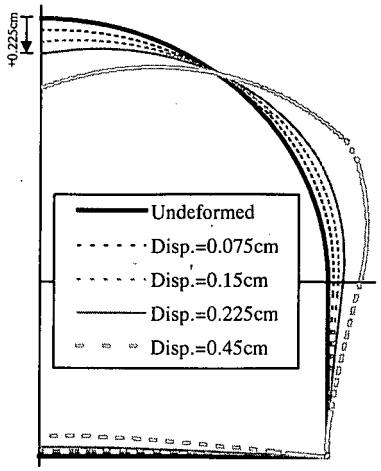

Fig.10 Deformation in case of t12_012_w2

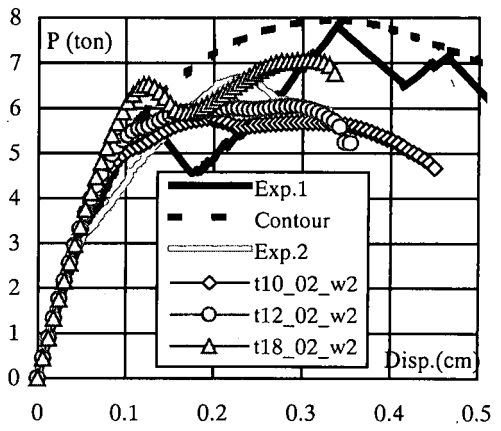

Fig.11 Load-displacement relation with different concrete tensile strength

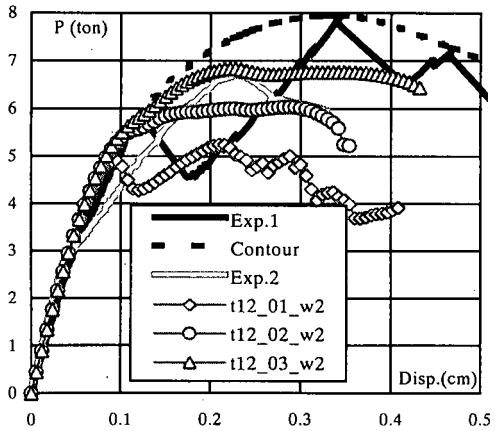

Fig.12 Load-displacement relation of different fracture energies

consistent with the experimental ones. Although weak elements are also given in t12_02_w2_p2, the crack does not propagate further and is still widely distributed at the outside of sidewalls. It means that the stress redistribution after crack occurs at position ④ does not result in further crack propagation. A deformation of tunnel lining of the basic case t12_02_w2 is shown in **Fig.10**.

(2) Effect of Concrete Tensile Strength

Due to the randomness and different conditions during pouring the concrete specimens, such as temperature, humidity, drying time, component ratio and the scale of structures, the strength of concrete, especially the tensile strength may vary. It also has significant influence to the structural response of the tunnel linings. In this section, 3 cases of tunnel linings with different concrete tensile strengths, f_t=10, 12 and 18kgf/cm^2, are compared, with the fracture energy G_f^I=0.2kgf/cm.

From the numerical results, it can be seen that tensile strength mainly affects the elastic loading stage and the structural load carrying capacities, as shown in **Fig.11**. Therefore, the guarantee on tensile strength of concrete is considered to be important in plain concrete tunnel lining. It is found that tensile strengths used in simulation are lower than that of concrete sample, $f_t=0.5f_c^{2/3}$=20.5kgf/cm^2, in which the case of f_t=18kgf/cm^2 is overestimated in elastic loading stage and the case of f_t=12kgf/cm^2 lies in the scope of two experimental results. Hence, the tensile strength of concrete sample can not completely reflect the one of 1/3 scale model tunnel lining specimen. In this point of view, the tensile strength of large scale concrete tunnel lining specimens seem to be lower, compared to the one obtained from sample strength test. For the high tensile strength tunnel lining, the first load peak followed by a degradation indicates complete crack at position ①. The degradation behavior that seems similar to the results of Exp.1 will be studied in future work.

(3) Effect of Fracture Energy

Many researchers have considered the fracture energy, G_f^I, as a material property, which is defined as the amount of energy required to create one unit of area of a mode I crack. But due to the lack of information of this property, herein, 3 cases with fracture energy G_f^I=0.10, 0.20 and 0.30kgf/cm are studied. The concrete tensile strength is kept

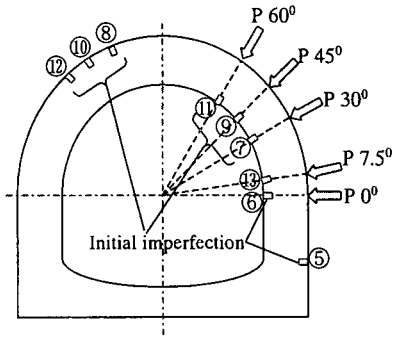

Fig.13 Load cases with different positions

constant, as f_t=12kgf/cm^2.

Different from the effect of concrete tensile strength, the fracture energy more likely affect the deformation behavior after crack initiation and structural strength, in **Fig.12**. The higher the fracture energy is taken, the more ductile the structure shows and the higher structural strength can be archived. From the simulation above, it is inferred that more fracture energy would be needed to match the peak load of experiment result in Exp.1, though the fracture energy G_f^I=0.30kgf/cm in case of t12_03_w2 is normally considered as a large value for concrete. But it should be larger than G_f^I=0.10kgf/cm.

(4) Effect of External Load Positions

In the experiment, only one load case was considered, where the load was acted vertically down at the outside of crown. However, the real load conditions due to ground lining interaction or earthquake may be more complicated. They can act in different directions and at different positions. Hence, a case study of various load conditions could be helpful to the understanding of real cracking behavior of tunnel linings.

Beside the basic case according to the experiment, other 5 cases are simulated, with load direction inclined to x axis with angle 0^0, 7.5^0, 30^0, 45^0 and 60^0, respectively. In the similar way, the weak elements are given at the positions where the stress level is relatively large, as marked in **Fig.13**.

Fig.14 shows the analytical results of crack patterns. The cracks are mostly localized at the positions where the weak elements are given. For the cases with load direction of 30^0, 45^0 and 60^0, cracks occur and propagate at the left inside of corner even though the weak element is not given there, whereas for the load cases of 0^0 and 7.5^0, the

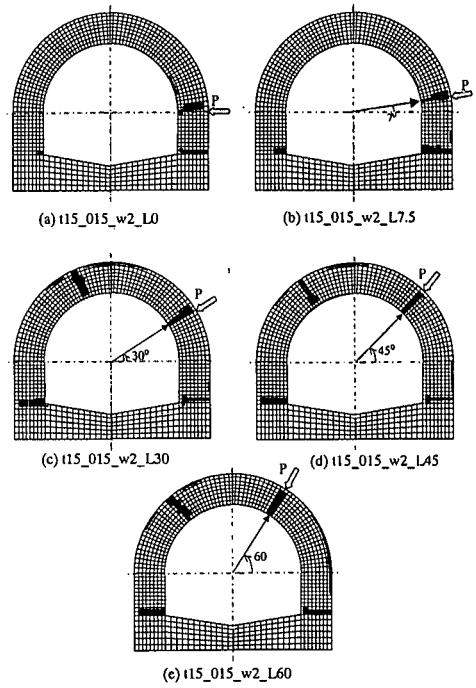

Fig.14 Crack patterns under various load conditions

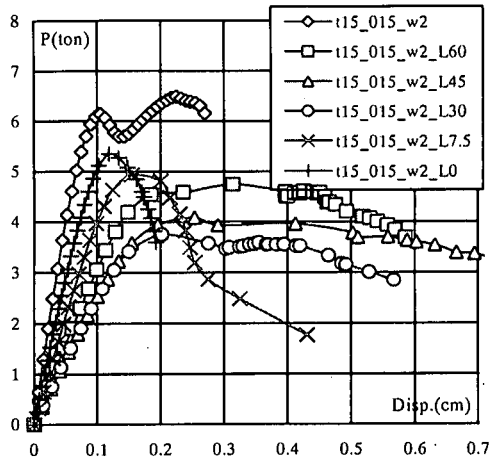

Fig.15 Load-displacement curve of different load directions

cracks occur mainly at the load positions and the right inner corner of bottom.

It means the left inner corner is a critical position which is easy to crack under a load in the direction larger than 30^0. From load-displacement curve in **Fig.15**, it is found that the tunnel lining has the maximum structural strength and stiffness under vertical direction load. With the variation of load direction from 90^0 to 30^0, both structural strength

and stiffness decrease, but the deformation at load point seems to increase, in which the horizontal displacement component is much larger than the vertical one. However, when the load direction changes to 7.5^0 and 0^0 the structural strength and stiffness tend to increase again. It can be concluded that the tunnel lining becomes most flexible and least load resistant when the load is acted in a direction inclined to x axis between 7.5^0 and 30^0.

(5) Size Effect

The size effect in brittle concrete structures is a well known phenomenon. Since one objective of our numerical simulation as well as the experiments is to find a proper method to evaluate the structural response of full size tunnel linings from the scale model specimens, the size effect should be discussed. The structural strength of different size tunnel linings might be not simply size-proportional. According to Bazant's research[5], the average strength was found to decline with the increase of size and finally approximate to a constant. In some literature[6], it was recognized that fracture energy might be also influenced by the specimen size. And it was realized that, for the relatively larger size specimen, the fracture energy of concrete may be bigger due to large aggregate size. But such an effect was not found in other cases.

In this section, the numerical results of 5 different sizes of scale model tunnel linings, with the scaled ratio 1/1, 1/3, 1/10, 1/20 and 1/30, are compared to find the size effect law. It is assumed that the fracture energy G_f^I is kept unchanged, as well as the concrete tensile strength f_t, in the simulations

The load-displacement curve is shown in **Fig.16**. The small size tunnel lining tends to be more durable with relatively large deformation. To find out the size effect on structural strength, the ratio of the structural strength P_{max} to the characteristic size r, defined as the average strength, is compared, as shown in **Table 2**, in which the characteristic size r is taken as the inner radius of the tunnel lining for each size. It is found that the ratio decreases with increasing the specimen size. And it can be predicted that the value of ratio P_{max}/r for tunnel lining of larger size will be much smaller and finally approximate a constant, but not continuously drop to zero, as shown in **Fig.17**.

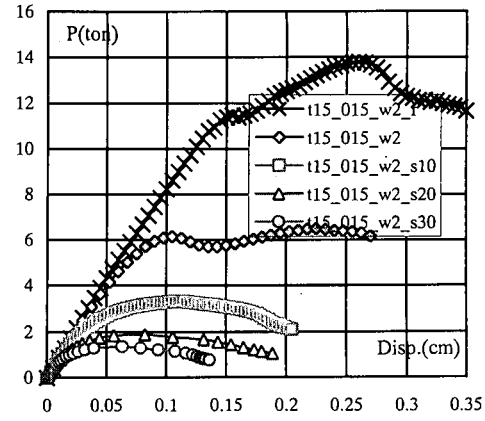

Fig.16 Load-displacement curve of size effect

Table 2 Size effect on structural strength

Cases	Structural strength P_{max}(ton)	Characteristic size r(cm)	Ratio P_{max}/r (ton/cm)
t15_015_w2_f	13.8	450	0.0307
t15_015_w2	6.49	150	0.0433
t15_015_w2_L10	3.3	45	0.0733
t15_015_w2_L20	1.888	22.5	0.0839
t15_015_w2_L30	1.362	15	0.0908

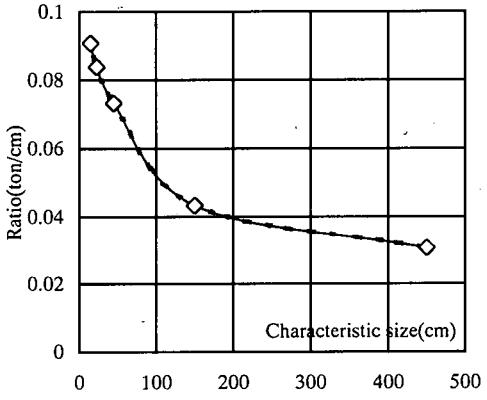

Fig.17 Size effect on structural strength

(6) Effect of Soil Mass Constrain

For the real tunnel linings, the load conditions include not only concentrating force as simulated in experiment, but also the constrain from outside soil of the tunnel linings. For simplicity, the gravity of soil mass is neglected. The soil mass constrains the outward deformation of the tunnel lining. In our numerical simulation, it is approximated by a series

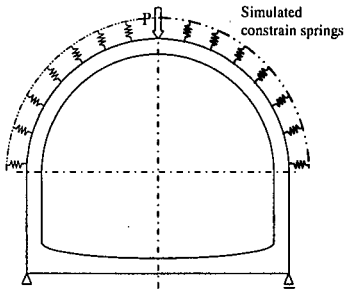

Fig.18 Simulation of soil mass constrain

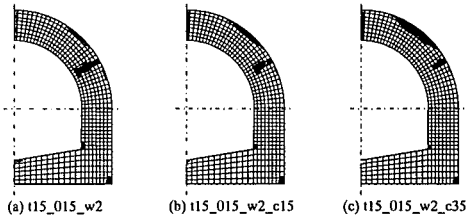

Fig.19 Crack patterns with and without constrain

of spring elements outside the semicircle sidewalls, which are assumed to resist only compression and to have zero stiffness when subjected to tension, in **Fig.18**.

Because of the difference of soil mass density outside the tunnel linings, the constrain effects may be also different. In the simulation, this difference is reflected in the stiffness of spring elements. Two values of constrain spring stiffness with $c=15kgf/cm^2$ and $c=35kgf/cm^2$ are used.

From the numerical results in **Fig.19** and **Fig.20**, it can be seen that the case t15_015_w2_c35 with high spring stiffness shows high structural strength. The crack propagation and localization are not obvious. It means that the soil mass constrain outside of the tunnel linings prevents the cracking development and is beneficial to the increase of structural stiffness and strength.

5. CONCLUSION REMARKS

By using the smeared crack model, numerical simulation has been done to investigate the cracking behavior of 1/3 scale model of plain concrete tunnel lining. From the case studies in several aspects it can be concluded that:

(1) The crack localization at inside of crown and outside of sidewalls significantly affects the

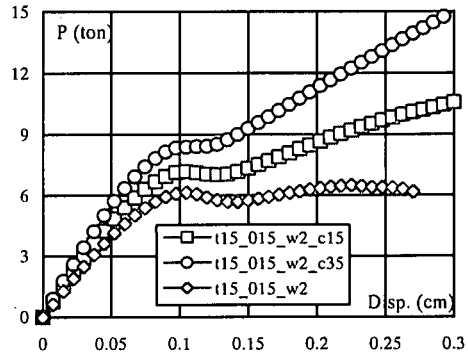

Fig.20 Load-displacement curve with and without soil mass constrain

structural strength of tunnel lining.

(2) The parameter studies of concrete tensile strength and fracture energy shows that the tensile strength mainly determine the scope of elastic loading stage while the fracture energy mainly affect the structural deformation in nonlinear loading and structural strength.

(3) Tunnel lining behaves the different responses under various load conditions, and has the low structural stiffness and strength with a load acted in a direction between 7.5^0 and 45^0 inclined to horizontal direction.

(4) The structural strength of tunnel linings is not simply size-proportional. It is predictable that the ratio of structural strength to characteristic size decreases with increasing the size, and tends to approximate a constant.

(5) The tensile strength of concrete materials seems to be degraded with the increase of structure size. This may be seen from the difference between the tensile strength of concrete sample test and the one used in numerical simulation, by which the analytical result agree well with the experimental one.

(6) A homogeneous soil mass constrain outside the tunnel lining may prevent the crack localization and development, thus increase the structural stiffness and strength.

(7) As to the smeared crack model, it is basically regarded to be applicable to simulate the cracking behavior of tunnel linings, especially when weak elements, as initial imperfection, are applied for capturing the crack localization, even with a gentle stress gradient in a structure.

Effective evaluation of cracking behavior in

tunnel lining can provide designers and engineers helpful information on how to design the new tunnels, to diagnose and repair the existing tunnels in service to extend their service life efficiently as much as possible. This study is still in the initial stage. More intensive researches, such as the cracking behavior under difficult load conditions including the distributed load and other structural modes, need to be carried from now on.

REFERENCES

1) Asakura, T., Ando, T., and Kojima, Y. : Analysis on the behavior of tunnel lining Experiments on double track tunnel lining, *QR of RTRI,* Vol.33, No.4, 1993.
2) Pottler, R.: Non-reinforced inner linings of tunnels: Numerical model-safety philosophy with different nonlinear elastic material models, *Proc. of Int. Conf. on Computer Aided Analysis and Design of Concrete Struc.*, Nenad, B. and Herbert, M., eds., Vol.1, pp.683-694, 1990.
3) de Borst, R. and Nauta, P. : Smeared crack analysis of reinforced concrete beams and slabs failing in shear, *Proc. Int. Conf. on Computer Aided Analysis and Design of Concrete Struc.*, Damjanic, F. et.al eds., Part 1, Prineridge Press, Swansea, pp.261-273, 1985.
4) Asakura, T., Ando, T. and Kojima, Y. : Experiments of inner reinforced tunnel linings, *QR of RTRI,* 1998.
5) Bazant, Z.: Size effect in blunt fracture: concrete, rock, metal, *J. of Eng. Mech. ASCE*, Vol.110, No.4, pp.518-535, 1984.
6) Wittmann, F.H., Mihashi H. and Nomura, N. : Size effect on fracture energy of concrete, *Eng. Fracture Mech.*, Vol.35, No.1, pp.107-115,1990.

(Received November 4, 1999)

分布クラックモデルによるコンクリートトンネル覆工のひび割れ性状及び破壊挙動に関する数値解析的研究

殷　峻・呉 智深・朝倉 俊弘・太田　裕之

複雑なひび割れ特性を有するコンクリートトンネル覆工は，他のコンクリート構造物と違って厳密な設計がなされておらず，またその健全性診断はひび割れ性状に寄らざるを得ないのが現状である．本論文は，分布クラックモデルを導入した非線形有限要素法によりコンクリートトンネル覆工のひび割れ特性や破壊挙動を解析・検討したものである．実験現象や結果に基づき，1)内部初期亀裂の位置変化，2)コンクリート引張り強度の変化，3)破壊エネルギーの大きさ，4)外部荷重の変化，5)寸法効果，6)土圧の作用などについて因子解析を行い，トンネル覆工の特性、破壊挙動および構造解析手法自身に及ぼす影響を究明した．本研究により得られた結果はトンネル覆工的設計，構造診断および補強対策に有用な知見を与えると考えられる．